27. Modeling of Coastal Waves and Hydrodynamics

Patrick J. Lynett, James M. Kaihatu

This chapter presents an overview of the available methods for modeling coastal waves. First, an overview of the relevant coastal processes, from shoaling to turbulent mixing, is provided to establish a basis to compare the various modeling approaches. The bulk of the discussion centers on modeling wind waves and includes a brief overview of the linear and analytical theory available to quantify coastal transformation, and then follows with a summary of spectral and phase-resolving approaches. Modeling long waves is discussed next, with a focus on tsunami simulation. Finally, the chapter summarizes techniques to couple the various models and reviews recent advances in the topic.

As an ocean surface wave enters the coastal zone, broadly defined here as the water landward of the continental shelf or some other depth transition, interaction with the seafloor and currents causes significant transformation. Waves will first start to feel the bottom when the depth (h) to wavelength (L) ratio is less than $1/2$, and waves are considered to be in shallow water, where the effects of the bottom are strong, when this ratio dips below approximately $1/25$. Two-dimensional (2-D) variations in the seafloor can lead to wave focusing due to the effects of refraction. Wave shoaling causes the wave amplitude to grow and the wavelength to shorten, steepening the wave front until the wave breaks.

Depending on the properties of the incoming wave, nonlinearities in the wave behavior are important for some distance before breaking and through the surf zone. Shallow water nonlinearity is governed by the wave height to water depth ratio; as the ratio gets larger, it is expected that nonlinearity becomes increasingly important. From this definition, it is clear that nonlinearity must be important near breaking, as this is the point when the wave height is similar to the depth. Nonlinearity in the coastal zone can change the speed at which a wave travels, where it breaks, and how it interacts with currents.

Nonlinear waves in the coastal zone also induce a net mass transport in the direction of the wave. This net mass transport is due to wave radiation stress, which is name given to the net positive momentum flux in the direction of wave propagation, and leads to wave-induced currents. Currents moving parallel to the shoreline are termed alongshore currents and are primarily responsible for alongshore sediment movement. These currents can generate instabilities, often driven by alongshore bathymetry variation, which can manifest as strong rip currents and shallow turbulent coherent structures. Such features induce high horizontal shear on the flow, and lead to significant horizontal and vertical mixing.

When designing coastal structures, engineers are often most concerned with extreme event loads. Here, extreme events may be storm surges and the accompanying storm waves or tsunamis, for example. It is a present challenge for coastal engineers to determine these extreme event loads, as there is currently no accepted design code for extreme wave loads. Furthermore, the sea level rise associated with climate change

has the potential to increase peak water levels during storms [27.1], also implying that wave energy may penetrate further inshore. The engineer is left with many different options to quantify the wave properties in the coastal zone, from overly simple methods to impractically complex numerical tools.

Relative to many engineering disciplines, the use of numerical coastal wave models for design is new. Many analyses still rely on the simple linear wave methods described in the following section. The usage of large-scale spectral wave models has become commonplace, as these models are efficient and well tested. Currently, it is less common to go to detailed phase-resolving models in engineering practice. These models provide a wave-by-wave resolution of the coastal dynamics, and can provide insight on a small spatial scale. Such insight is important when trying to, for example, accurately estimate wave overtopping of a coastal levee or wave impact loads on a structure. The following sections of this paper will outline the various approaches, providing a brief literature review and theoretical background.

27.1 Wind Wave Modeling

There is a wide range of useful techniques for estimating wind wave properties in the nearshore; the choice of which technique to use depends on limiting factors such as the resources available, the precision required in the result, and the physical properties of the waves themselves. The types of approaches discussed in this section have both highly variable physical approximation as well as computational demand; these two factors often have an inverse behavior. It is the purpose of the following presentation to outline the main types of coastal modeling options, providing theoretical background, numerical modeling schemes, and typical applications.

27.1.1 Linear, Analytical and Semi-Empirical Approaches

The simplest methods for estimating coastal wave properties utilize linear potential wave theory. While this theory is covered comprehensively in many textbooks [27.2], the most relevant equations are given here. Additionally, this presentation will serve to establish the basic variable quantities used in coastal hydrodynamic modeling. The free surface elevation η for a single frequency component is given by

$$\eta = \frac{H}{2}\cos\theta \,,$$

where H is the wave height equal to twice the wave amplitude a. For one horizontal dimension and constant depth, θ is the wave phase function given by

$$\theta = kx - \omega t \,,$$

where k is the wave number, x is a horizontal coordinate, ω is the angular frequency, and t is time. In general terms, k and x can be vector quantities when directional waves are considered. Wavenumber and angular frequency are related to other important physical quantities

$$k = 2\pi/L, \quad \omega = 2\pi/T, \quad f = 1/T \,,$$

where L is the wavelength, or horizontal distance between two successive crests or troughs, T is the wave period, and f is the wave frequency. The linear dispersion relation provides the connection between wave frequency and wavelength

$$\omega^2 = \mathrm{g}k\tanh(kh) \,,$$

where g is gravity, h is the local water depth, and the fluid is assumed inviscid. Expressions for fluid velocity and pressure under the wave can be found in textbooks, and will not be repeated here. Linear wave theory predicts closed, elliptical orbits of fluid particles under waves, and, therefore, no net mass transport.

In the limited case of very shallow water, where the ratio of water depth to wavelength approaches zero, simplifications can be made to the full linear potential theory discussed above. The dispersion relation reduces to

$$\omega^2 = \mathrm{g}hk^2 \,,$$

which yields a wave speed c of

$$c = \frac{\omega}{k} = \frac{L}{T} = \sqrt{\mathrm{g}h}$$

and a horizontal fluid velocity u of

$$u = \frac{H}{2}\sqrt{\mathrm{g}/h}\cos\theta \,.$$

These expressions should be applied only in the case of a very long wave, such as for tides, tsunamis, and swell

waves in very shallow water. However, even outside these cases, quick wave property calculations based on the above will still provide a useful preliminary reference point for shallow water wind waves.

Linear wave transformation in shallow water includes the effects of shoaling, refraction and diffraction, and can be expressed in the general form

$$\frac{H}{H_o} = K_S K_R K_D \,,$$

where H represents the wave height at some coastal location, H_o the height at some offshore location, K_S is the shoaling factor, K_R is the refraction factor, and K_D is the diffraction factor. Assuming no dissipation of energy during propagation, the conservation of wave power between any two locations in the propagation path gives the shoaling coefficient

$$K_s = \sqrt{\frac{n_o L_o}{nL}} \,,$$

where

$$n = \frac{1}{2}\left[1 + \frac{2kh}{\sinh(2kh)}\right] .$$

This n value varies from 0.5 for a deep water wave to 1.0 for a shallow water wave. It is remarked that the basic linear theory presented here does not include bottom reflection or bottom dissipation, and can thus be applied between any two points regardless of the bathymetry between these two points. However, the theory implicitly assumes inviscid propagation and a mildly sloping bottom, and this must be satisfied at a minimum for the shoaling estimation above to be physically appropriate.

Wave refraction is the process of wave crests bending due to propagation-normal variations in bathymetry. Wave crests will bend *into* shallow water regions as the propagation speed slows in such regions, with the refraction coefficient

$$K_R = \sqrt{\frac{\cos\alpha_o}{\cos\alpha}} \,,$$

where α is the angle of incidence relative to the shoreline or some prescribed depth contour, and can be found using Snell's Law

$$\sin\alpha = \frac{c}{c_o}\sin\alpha_o \,.$$

This relation may only be used in simple bathymetries with shore-parallel bottom contours. In more complex regions, modified forms of Snell's law can be used to create wave rays, which were commonly used in the twentieth century to show wave paths and outline possible areas of wave focusing and de-focusing. These techniques have been displaced by numerical methods, some of which are discussed in later sections of this chapter. There is no general equation for the diffraction coefficient. The engineer should reference the numerous diffraction diagrams that can be found in the Coastal Engineering Manual CEM) [27.3], which plot K_D surfaces for various combinations of breakwater configurations and incident wave directions.

Once the wave reaches the break point, the coastal transformation equation given above can no longer be used, and some other approach must be used to cap the wave height. A common engineering approach is the introduction of the breaker index, which is the ratio of the breaking wave height to the local water depth. For a given wave period and bathymetry slope, a breaker index can be estimated. Once the shoaling and refraction analysis estimates a wave height to depth ratio that exceeds the breaker index, it is assumed the wave starts to break; this is the break point. Breaking is then usually assumed to be *depth limited*, meaning that the breaker index remains constant as the water depth decreases onshore. The difficulty in this approach is determining a reliable estimation of the breaker index. There are numerous different equations for this index; the most common are found in the CEM. For waves shoaling over a very steep slope, the breaker index can be greater than 1.0, while for waves breaking over an essentially flat bottom, the breaker index may be lower than 0.4 [27.4]. A commonly assumed value for the breaker index found in engineering studies is 0.78; this is derived from the maximum theoretical solitary wave height, and its physical relevance to random coastal wind wave breaking is questionable.

For studies that seek to use straightforward analysis methods but also provide an estimate of the wave height envelope across a cross-shore beach profile, the energy flux method [27.5] is a useful tool. Here, it is assumed that the spatial rate of change of wave energy flux F is due to some dissipation function φ

$$\frac{\mathrm{d}F}{\mathrm{d}x} = -\varphi(x) \,.$$

The dissipation function is driven by breaking and is proportional to the difference between the local wave energy flux and some *stable* energy flux for the local depth. Determination of a stable energy flux is, similarly to the determination of a breaker index, difficult for a wide range of conditions. Commonly used models for the dissipation function include [27.6] and [27.7], which are both established for random wave break-

ing. Note that outside the breaker zone, where the left-hand side of the above equation is zero, the energy flux method will reduce to a linear shoaling model. This wave transformation model has been adopted by a number of large-scale morphology change simulators, which require a good estimate of the breaker location and resulting longshore currents for large horizontal areas. However, this approach has been largely displaced by more recent numerical tools, which can better include directionality, dissipation, and nonlinear effects. Some of these tools are discussed in the following sections.

27.1.2 Spectral Modeling: Phase-Averaged and Phase-Resolving Approaches

In the open ocean, wind wave generation and propagation are typically described using phase-averaged spectral models. These spectral models determine spatial and temporal changes in the wave spectrum, or the wave energy as a function of frequency and direction. A spectral energy balance is derived, accounting for wave growth, propagation, and dissipation based on wind energy input, whitecapping, and bottom friction. Examples of such models are WISWAVE (wave information study wave model) [27.8], WAVEWATCH III [27.9], and WAM (wave model) [27.10]. These models are highly developed for open ocean waves, but do not account properly for coastal effects such as shallow water wave–wave interactions and depth-induced breaking [27.11]. They output a directional spectrum, which can then be employed as boundary conditions in a coastal zone model to simulate nearshore propagation. For example, WAM could be coupled with SWAN (simulating waves nearshore) [27.12], a coastal spectral model, to estimate the spectral evolution from deep to shallow water [27.11]. However, even coastal spectral models only crudely approximate dynamic nearshore phenomena, due to the inherent approximations such as phase-averaging, weak nonlinear effects, and no diffraction.

In its most general form, the spectral wave action density balance equation is given by

$$\frac{D_w(N)}{Dt} = \frac{S}{\omega} ,$$

where N is the time-dependent wave action density, or energy density divided by frequency, defined for an individual frequency; the total derivative $D_w(N)/Dt$ is taken in the direction of wave motion, and S represents any external source or sink acting on the conservation volume for which the total derivative is taken. S by definition includes forcings such as those of wind and viscous dissipation, such as whitecapping, wave breaking, and bottom friction. If the nonlinear advection terms are neglected from the total derivative, then S must also include nonlinear energy transfers among the various frequencies. Expanding the above balance equation, and including the terms of coastal importance, we have

$$\begin{aligned}\frac{\partial N}{\partial t} &+ (\text{linear energy transfers}) \\ &= \frac{S_{\text{bottom friction}}}{\omega} + \frac{S_{\text{breaking}}}{\omega} + \frac{S_{\text{whitecap}}}{\omega} \\ &\quad - \frac{S_{\text{wind input}}}{\omega} - (\text{nonlinear energy transfers}) ,\end{aligned}$$

where the mechanism of each source/sink S term is given in its subscript, and the nonlinear energy transfer term represents energy transfer from one frequency to a different frequency. For example, the bottom friction sink is most commonly expressed in the Joint North Sea Wave Project (JONSWAP) form [27.13]

$$S_{\text{bottom friction}} = -C_b G(f) E ,$$

where C_b is a bottom friction coefficient dependent on local wave and bottom conditions, G is the *functional form* of the sink and is dependent on the frequency, and E is the local energy density. G has the physically reasonable form of being large at low frequencies (high dissipation in shallow water) and approaches zero (no dissipation) in the deep water region. The breaking dissipation source function is restricted by breaker-index uncertainties similarly as discussed with the linear modeling in the previous section. However, due to the ability of these coastal spectral models to include nonlinearity and approximate dissipation, they have been shown to be excellent predictors of wave height transformation for a wide range of physical configurations. It is reasonably stated that, if the user is not interested in detailed wave-by-wave breaking estimation, runup, infragravity waves, three-dimensional (3-D) flow profiles, and turbulent dynamics such as rip currents and coastal eddies, then coastal spectral models are the most efficient and accurate option available. For a further discussion and a nice review of state-of-the-art spectral modeling methods, the reader is directed to [27.14]. Figure 27.1 shows a result from the SWAN model [27.12], with an improved numerical scheme for the geographical propagation terms [27.15], applied to the area surrounding Santa Rosa and San Miguel Islands in the Southern California Bight. The extreme refraction around the islands served as a stringent test of the model; the single-peaked incident wave spectrum (Fig. 27.1c) has split into two discrete spectra at the location of the measurement station between the two islands.

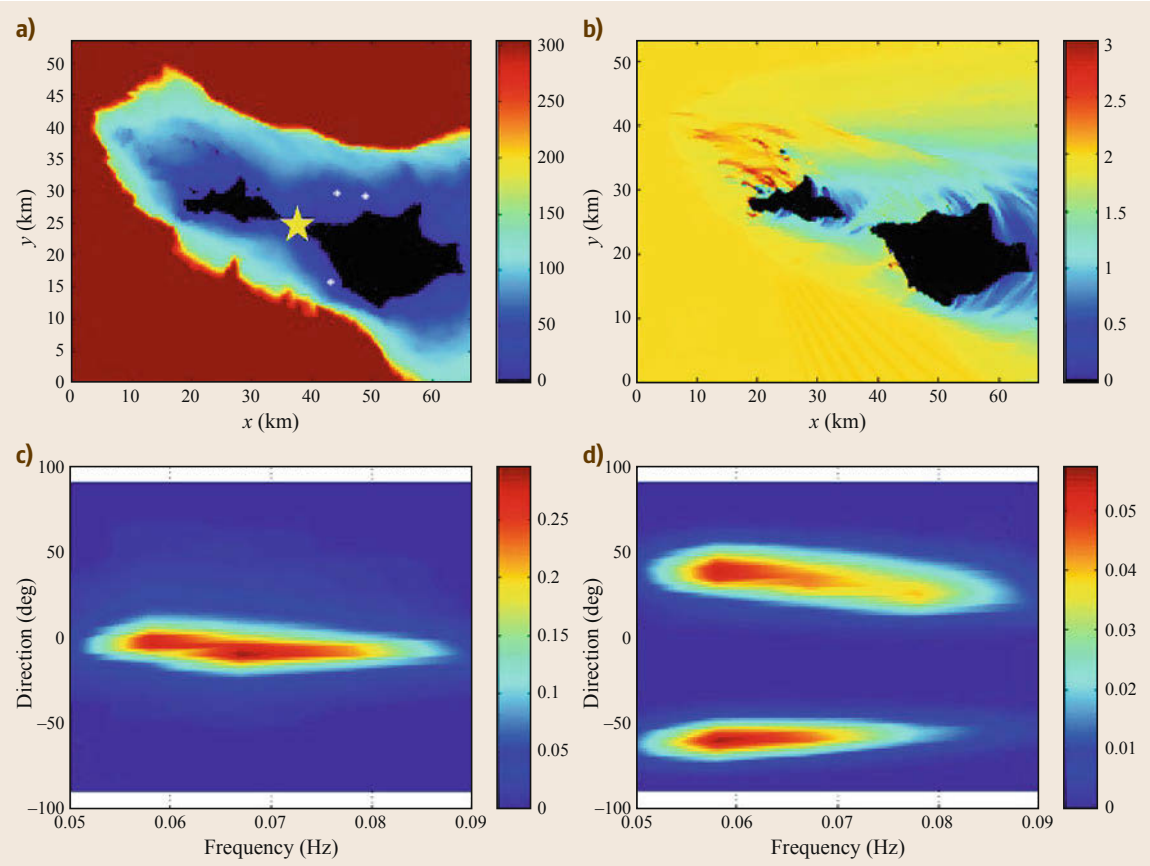

Fig. 27.1a–d SWAN simulation of wave refraction around San Miguel and Santa Rosa Islands in the Southern California Bight. **(a)** Bathymetry (in m) and pressure gage locations (*white dots*) near San Miguel (*left*) and Santa Rosa (*right*) Islands; location of pressure gage #10 denoted with a *star*. **(b)** Significant wave height (in m) on January 14, 1992 at 2300 Pacific Standard Time. **(c)** Incident swell wave spectrum measured offshore of Southern California Bight (January 14, 1992 at 2300 PST) and applied to the left and upper boundaries of local model domain shown in **(a)**; zero degrees denotes waves approaching from due west, while +90 degrees denotes waves approaching from due north. **(d)** Swell wave spectrum output at location of pressure gage #10

Modelers looking to perform phase-resolving simulations of waves from intermediate depths to the shoreline have few options. Well-established models such as SWAN and STWAVE (steady state spectral wave model) [27.16] are phase-averaged models and do not directly provide time histories of free surface and velocity fluctuations due to waves. Mild-slope equation models, such as REF/DIF (refraction/diffraction model) [27.17], are phase-resolving models and are computationally practical to run in most cases. However, these models have restrictions that limit their use, such as weak diffraction effects, a lack of wave reflection, and the limitation to narrow banded spectrums, and higher-order nonlinearity is generally not captured [27.18].

An alternative approach to spectral phase-averaged modeling, which retains both shallow water nonlinearity and the periodic nature of waves, is nonlinear frequency-domain wave modeling [27.19–22]. In essence, these models are nonlinear extensions of phase-resolving nearshore linear refraction-diffraction models such as REF/DIF [27.17]; a relatively comprehensive account of these models is given in [27.23]. These models retain second-order nonlinearity via near resonant interactions (both subharmonic and superharmonic interactions) between triads of frequencies. The strength of the interactions is dictated by both the interaction coefficients and the phase mismatches between the complex amplitudes of the spectral components. These models have been improved to include wide-

angle parabolic propagation [27.24] and interaction effects among triads of longshore wavenumbers [27.22, 25]. Several models also contain a dissipation mechanism representing spectral wave breaking, consisting of a lumped parameter breaking description [27.7] coupled with an adjustable distribution of dissipation over the frequency range. The distribution is an adjustable balance between a frequency-independent weighting of dissipation and one that is weighted as frequency squared. The latter distribution was shown by *Kaihatu* et al. [27.26] to be an inner surf zone asymptote of the dissipation dependence on frequency. Smoothed versions of these phase-resolving models that treat triad interactions in terms of averaged bispectral quantities [27.22, 25, 27] have also been developed; these models are closer akin to the phase-averaged spectral models discussed previously.

27.1.3 Depth-Integrated and Boussinesq-Type Approaches

While frequency domain models are advantageous due to their relatively small computational demand, a significant effort in the nearshore wave model community towards developing phase-resolving, time domain Boussinesq models has occurred in the past decade. Assuming that both nonlinearity and frequency dispersion are weak and are of the same order of magnitude, *Peregrine* [27.28] derived the *standard* Boussinesq equations for variable depth in terms of depth-averaged velocity and free surface displacement. Numerical results based on the standard Boussinesq equations or the equivalent formulations have been shown to give predictions that compared quite well with field data [27.29] and laboratory data [27.30, 31].

As mentioned above, the standard Boussinesq equations are derived based on an assumption between the nonlinearity of the wave, $\varepsilon = a/h$, and the frequency dispersion of the wave, $\mu = kh$. The precise relation of these parameters comes from a nondimensionalization of the full potential flow equations using a shallow water scaling and is given by

$$O(\epsilon) = O\left(\mu^2\right) \ll 1 \,,$$

which is the *true* Boussinesq assumption as related to nonlinear long surface waves. With this assumption, nonlinear two-dimensional-vertical potential flow can be reduced to the one-dimensional 1-D-horizontal equation set for a wave over constant water depth as

$$\text{continuity:} \quad \eta_t + (\eta u)_x + h u_x = 0 \,,$$

$$\text{momentum:} \quad u_t + g\eta_x + u u_x - \frac{1}{3} h u_{xxt} = 0 \,,$$

where the subscripts represent partial derivatives and u is the depth-averaged horizontal velocity. The nondispersive, shallow-water wave equations are easily extracted from this equation set by neglecting the last term ($\frac{1}{3} h u_{xxt}$) on the left-hand side of the momentum equation; it is this single term that adds dispersion to the shallow water base.

The mathematical effect of the additional dispersive term can be quantified by examining the linear form of the standard Boussinesq equations given above and substituting in the linear wave solution form

$$\eta = \eta_o e^{i\theta} \,, \quad u = u_o e^{i\theta} \,, \quad \theta = kx - \omega t \,.$$

After some algebra, the dispersion relation of this approximate equation set can be expressed as

$$\omega^2 = \frac{g h k^2}{1 + \frac{1}{3}(kh)^2} \,,$$

which is also the $[0, 2]$ Pade approximation of the full linear dispersion relation given in the Linear Wave Approaches above (Sect. 27.1.1). In the practical sense, this single additional term in the momentum equation allows for accurate linear propagation of waves up to $kh \approx 0.5$, which is approximately a fivefold increase in applicability compared to the shallow water model, using the same accuracy thresholds in phase and group velocity [27.32].

As it is required that both frequency dispersion and nonlinear effects are weak and of the same order, the standard Boussinesq equations are not applicable to very shallow water depth, where the nonlinearity becomes more important than the frequency dispersion, nor to the deep water depth, where the frequency dispersion is of order 1. The standard Boussinesq equations break down when the depth is greater than $\approx 1/10$ of the wavelength. For many engineering applications, where the incident wave energy spectrum consists of many frequency components, a lesser depth restriction is desirable. To extend the applications to shorter waves (or deeper water depth) many modified forms of Boussinesq-type equations have been introduced [27.22, 33, 34]. Although the methods of derivation are different, the resulting dispersion relations of the linear components of these modified Boussinesq equations are similar, and may be viewed as a slight modification of the $(2, 2)$ Pade approximation of the full dispersion relation for linear water waves [27.35]. It has been demonstrated that the *modified* Boussinesq equations are able to simulate wave propagation from intermediate water depth (the water depth to wavelength ratio is about 0.5) to shallow water including the wave–current interaction [27.36].

Despite the success of the modified Boussinesq equations in intermediate water depth, these equations are still restricted to weak nonlinearity. As waves approach the shore, the wave height increases due to shoaling, until they eventually break. The wave height to water depth ratios associated with this physical process violates the weakly nonlinear assumption. This restriction can be readily removed by eliminating the weak nonlinearity assumption [27.37, 38]. Numerical implementations of the highly-nonlinear, Boussinesq-type equations include FUNWAVE (fully nonlinear Boussinesq wave model) [27.38] and COULWAVE (Cornell University long and intermediate wave model) [27.39]. These models have been applied to a wide variety of topics, including rip and longshore currents [27.40, 41], wave runup [27.42], wave–current interaction [27.43], and wave generation by underwater landslides [27.42], among many others. Boussinesq models are steadily becoming a practical engineering tool. Directional, random spectra can readily be generated by the models, which capture nearshore evolution processes, such as shoaling, diffraction, refraction, and wave–wave interactions, with very high accuracy. The applicability of the Boussinesq models is limited by the fact that the models are fundamentally inviscid. The dissipation processes, such as breaking and bottom friction, must be parameterized in traditional Boussinesq models.

Recently, a number of *non-traditional* Boussinesq approaches have been developed, with the goal of including horizontal vorticity explicitly in the flow field. An attempt to include these dynamics under a breaking wave is found in [27.44], with further advances given in [27.45]. Integrated within a Boussinesq-type derivation, the stream function equation is used to determine the vertical variation of the velocity. This allows the inclusion of the vorticity generated by breaking. The breaking terms that appear as corrections to the momentum balance are a function of the amount of vorticity generated during the breaking process. This vorticity is obtained from the solution to the vorticity transport equation and has been shown to capture the flow field dynamics under a spilling breaker.

A similar attempt was made by *Kim* et al. [27.46] who included the viscous effects of a bottom shear, and the associated rotationality, directly in a Boussinesq-type derivation. While this leads to a far more complex equation model, it includes the physics necessary to simulate boundary shear and the complete coupling of these effects with a nonlinear, dispersive wave field. This model can predict the friction-induced changes to the vertical profile of velocity under weakly unsteady flow and can thereby provide good estimates of internal kinematics. It is also able to translate the bottom-created horizontal vorticity into a vertical vorticity field.

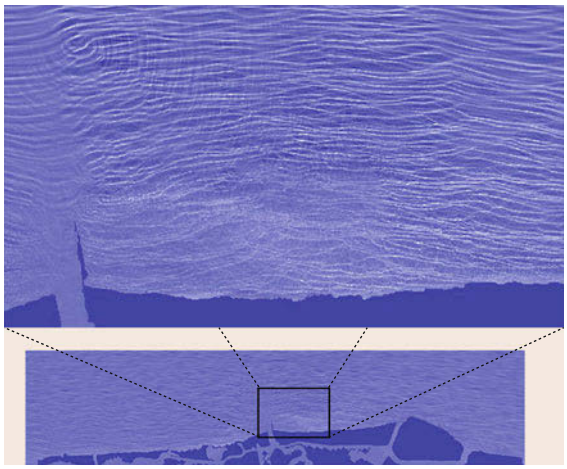

Fig. 27.2 Boussinesq simulation of waves near Freeport, TX. Resolution of the model is 5 m and the total spatial extent is $\approx 100\,\mathrm{km}^2$

Such a model is able to couple the dissipative and nonlinear effects of a bottom shear with a dispersive and nonlinear wave field. While this and similar recent advances allow the depth-integrated equations to model a wider range of physical processes, the computational cost for this inclusion is high [27.47]. In addition to the many individual calculations needed to quantify the various terms in these equations, since the model includes first to third-order spatial derivatives, it becomes necessary to resolve the leading order terms to fourth-order numerical accuracy. This leads to the requirement of a fourth-order spatial differencing and temporal integration scheme. Compared to an efficient shallow water solver, the highly nonlinear Boussinesq-type model can require 50−100 times more computational time for the same numerical grid and time step configuration. While this cost is relatively high, large domains can be tackled with parallel computing [27.48]. For an example of the possible scale of these simulations, see Fig. 27.2.

27.1.4 Navier–Stokes Equation-Based Approaches

Phase and depth-resolving surf zone hydrodynamic models, such as those that use the Reynolds-averaged Navier–Stokes(RANS) equations along with a turbulence closure and a robust free surface-tracking scheme, are an ideal alternative for simulation of complicated nearshore processes that involve breaking waves. In general, RANS-based models are capable of calculating turbulence energy and energy dissipation due to wave breaking and bottom friction. For example, in one of the RANS-based models, COBRAS (Cornell breaking wave and structure) [27.49–51], the two-

dimensional RANS equations are coupled with the k-ε turbulence closure and the volume of fluid (VOF) method for tracking free-surface position. This and similar models can adequately resolve the wave breaking process and its interactions with the seabed. An example of the types of output that this model provides is given in Fig. 27.3. RANS-based models have not yet been widely accepted into coastal science and engineering practice, as their computational cost is relatively high and the high-resolution physical output provided is often beyond what is needed by engineering standards of practice for design. Where these models are applied, it is usually for two dimensional vertical (2DV) transect studies, where, for example, details of wave breaking [27.52, 53], wave interaction with complex and/or porous structures [27.54], and fluid stresses and pressure distributions [27.55] are studied.

This general class of model is still not practically applicable, even in the academic sense, for simulating waves in 3-D coastal regions. 3-D solvers, using various turbulent closure schemes, are, however, becoming a common basis for large-basin numerical wave tanks. One of the more promising programs is OpenFOAM [27.56], which is an open-source and freely available computational fluid dynamics package. The flexibility in this package, and the ability to build off a significant body of previous computational fluid dynamics (CFD) work, makes it possible to apply the codes towards a variety of coastal modeling problems [27.57]. In the coming decade, it is anticipated that wind wave modeling will continually move towards the utilization of very high resolution, large eddy simulation (LES) tools, as this class of model is the main option for predicting vertical and turbulent structures which drive mixing and transport.

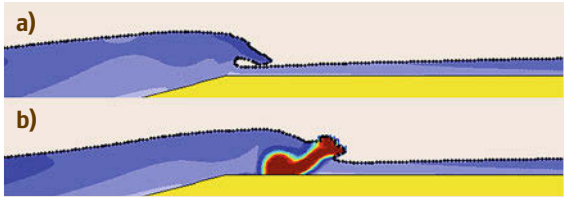

Fig. 27.3a,b Two snapshots from a RANS simulation of wind waves breaking on a shallow shelf. The *colors* indicate the intensity of turbulent kinetic energy. **(a)** shows the free surface and turbulent kinetic energy at moment of jet impingement on the free surface, and **(b)** shows the breaking wave a short time later.

27.2 Modeling Long Waves

A long wave is defined as having a wavelength much larger than the local water depth. Waves that commonly meet this requirement include tides, storm surges, and tsunamis. When the wave disturbance is considered to be *long*, it is reasonable to use the non-dispersive nonlinear shallow water (NSW) wave equations. The NSW equations can be derived in a number of different ways, but fundamentally all arise from an integration of the Euler or Navier–Stokes equations with an assumption of vertically-invariant horizontal velocity and hydrostatic pressure. Due to the simple and well-studied nature of the NSW equations, a wide variety of numerical schemes have been used to solve them.

Models that are used to examine tides and storm surges are often similar, if not the same model. Examples of this class of model include ADCIRC [27.58] and DELFT3D-FLOW [27.59], both of which have received widespread acceptance in the engineering community. These models need to include proper tidal forcing, wind stress for surge, and bottom friction in nearshore areas. Recently, circulation models have been coupled with nearshore short-wave spectral models, which provide a wave-induced water level and current forcing through radiation stress that is ingested by the circulation model [27.60]. This allows for a more complete nearshore simulation, as wave-induced currents become important near the surf zone. Of particular importance for accurate surge prediction is high resolution and accurate coastal bathymetry and topography, often down to 10 m or less. Therefore, as is a common challenge for simulation of long wave generation and evolution, a very wide range of scales must be simulated. Numerical approaches that can accommodate this issue, such as finite element meshing or grid nesting, must be adopted.

With the large number of deadly tsunamis in the past decade, tsunami simulation capabilities have increased relatively rapidly. Several tsunami computational models are currently used in the National Tsunami Hazard Mitigation Program, sponsored by the National Oceanic and Atmospheric Administration, to produce tsunami inundation and evacuation maps for the states of Alaska, California, Hawaii, Oregon, and Washington. The computational models include MOST (method of splitting tsunami), developed originally by researchers at the University of Southern California [27.61]; COMCOT (Cornell multi-grid coupled tsunami model), developed at Cornell University [27.62]; and TUNAMI-N2, developed at Tohoko University in Japan [27.63]. All three models solve the same depth-integrated and 2-D horizontal (2DH)

nonlinear shallow water equations with different finite-difference algorithms.

Successful simulation of tsunami propagation and accurate prediction of the arrival time and wave height at different locations rely on a correct estimate of the earthquake fault plane mechanism. Interplate faults in subduction zones are responsible for most of the large tsunamis in history. For interplate fault ruptures, the resulting seafloor displacement can be estimated approximately using linear elastic dislocation theory [27.64, 65]. For more sophisticated fault models, non-uniform stress-strength fields (faults with various kinds of barriers, etc.; [27.66]) are expected, so the actual seafloor displacement may be very irregular. Once the seafloor displacement has been determined, the initial ocean free surface profile is assumed to take the same configuration, based on the assumptions that the upward seafloor movement is impulsive and seawater is incompressible.

For a given source region condition specified by either the initial free surface elevations or a time history of sea floor displacement, existing models can accurately simulate propagation of a tsunami over a long distance, provided that bathymetry data exists. Figure 27.4 shows a snapshot of free surface elevation from a COMCOT simulation at 10 h and 44 min after the March 11, 2011 Japan tsunami. The shallow-water equation models by definition lack the capability of simulating dispersive waves, which could well be the dominating features in landslide-generated tsunamis [27.39] and for tsunamis traveling a long distance [27.67]. To address this issue of dispersivity, a different set of governing equations must be employed, or some manipulation of the numerical truncation error must be made.

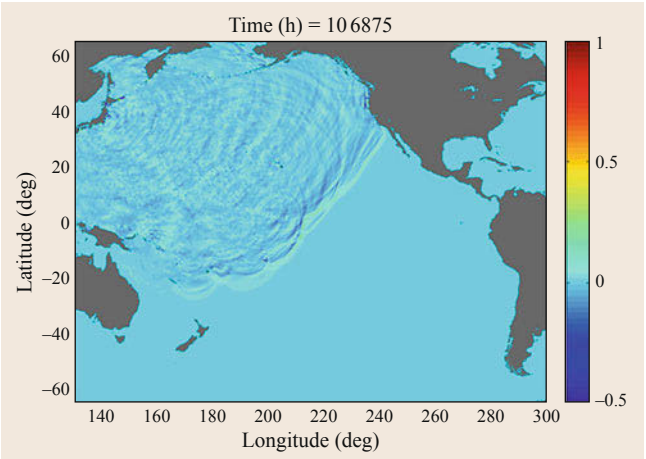

Fig. 27.4 Snapshot from tsunami simulation of the March 11, 2011 Japan tsunami

As a tsunami propagates into the nearshore region, the wave front undergoes a nonlinear transformation while it steepens through shoaling. If the tsunami is large enough, it can break at some offshore depth and approach land as a bore. Wave breaking in traditional NSW tsunami models has not been handled in a physically satisfactory manner. Numerical dissipation is commonly used to mimic breaking, and thus results become grid dependent. In Boussinesq models, this breaking is still handled in an approximate manner due to the fact that depth-integrated derivation does not allow for an overturning wave; however these breaking schemes have been validated for a wide range of nearshore conditions [27.68].

27.3 Coupled and Nested Techniques

As mentioned above, there have been recent successful attempts at coupling spectral wave models with circulation models, which allows for robust simulation of nearshore currents and the resulting transport. If one is interested in basin-scale simulation of wind waves with high coastal resolution, a natural coupling technique would be to use spectral wave information taken from a large-scale model, such as SWAN or STWAVE, to drive a detailed near-coast model, such as the Boussinesq model. Since these two models function in different dimensional space, the coupling between the two models is likely to be one way; meaning that information is given by the spectral model, but no information is received by the spectral model. The implementation of this coupling is straightforward, as it is with most one-way coupling methods, and has been used in a number of studies.

If examining transient wave phenomena or wave hydrodynamics on a fine scale, spectral models are of limited use. Of the two typical phase-resolving, depth-integrated models used in wave studies, the Boussinesq model can be considered a more physically complete (or at least a higher-order) approximation compared to the NSW. In coastal regions, where the water depth is very shallow and thus amplitude is large and wavelength becomes short, nonlinear and bathymetric interactions across a wide range of frequencies occur. These interactions can locally generate various shorter-crested, or dispersive wave components, even if the offshore forcing is considered a long wave. A well-known example is the transformation of a tsunami front into an undular bore. Thus, the nearshore is expected to be nonlinear and (possibly) dispersive, and a Boussinesq model is appropriate. However, the additional physics

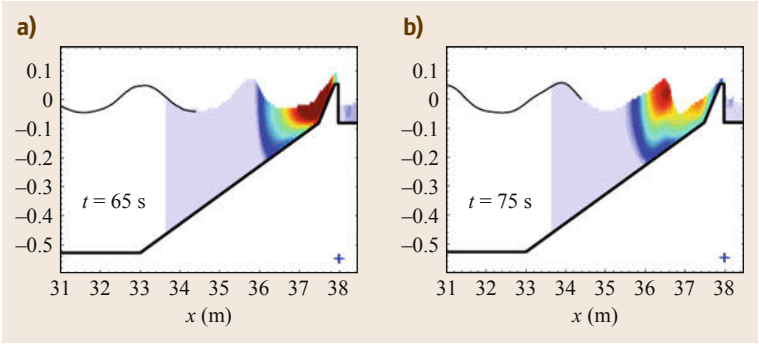

Fig. 27.5a,b Example hybrid Boussinesq-RANS setup; the Boussinesq domain stretches from $x = 0-34$ m and the RANS exists from $x = 34-39$ m. **(a)** shows an overtopping wave at the time of maximum speed on the front of the seawall, while **(b)** depicts the wave and turbulent kinetic energy during the downrush of water along the seawall

included in the Boussinesq approximation come with substantial computational cost, often making the model impractical for ocean basin scale simulations. If one wants to use the physical advantages of the Boussinesq model for a local region in the nearshore zone, it becomes necessary to couple that Boussinesq model with some other source of wave information for its boundary conditions. The obvious coupling choice would be the NSW, proven for both efficient and accurate basin scale tsunami prediction.

There are numerous challenges with this coupling, most notably that fact that the two approximations (NSW and Boussinesq) are different, and so there can be a physical mismatch across the coupling interface. Also, the NSW will typically have a low-order numerical solution approach (hence its computational efficiency), while high-order partial derivations in the Boussinesq model require a high-order scheme; matching these two schemes can also create numerical stability issues. Details regarding a coupling NSW-Boussinesq approach can be found in [27.69].

While Boussinesq models can provide a detailed description of the flow due to a tsunami, it can be necessary to use a model with even less restrictive physical approximations, and the ability to resolve very small-scale (sub meter) turbulent features, such as a 3-D Navier–Stokes model. A similar coupling argument as provided above for the Boussinesq can be made here for the fully 3-D model. Due to their high computational costs, full 3-D models would best be used in conjunction with a depth-integrated two-dimensional-horizontal model (2DH) (i. e., depth-integrated NSW or Boussinesq). While the 2DH model provides incident wave information, the 3-D model computes local wave–structure interactions. The results from 3-D models could also provide a better parameterization of small-scale features (3-D), which could then be embedded in a large-scale 2DH model. One-way coupling (using a NSW-generated time series to drive a 3-D model, but not permitting feedback from the 3-D model back into the NSW) is fairly straightforward to construct [27.70]. Two-way coupling, however, is difficult and requires consistent matching of physics and numerical schemes across model interfaces.

Sittanggang and *Lynett* [27.71] presented work on coupling of a Boussinesq model and 2-D Navier–Stokes model. The two models are two-way coupled, and so act as if they are a single model working on a continuous domain. In the coupling implementation, the Boussinesq model is applied in the non-breaking zone and the RANS model in the breaking/high-turbulence zone. The two models share a common domain interface for exchanging data, used as boundary conditions in the models. By coupling the two models, accurate large-scale wave simulation using a coarse grid and *simple* physics in the deep-to-intermediate water and fine grid and detailed physics in the nearshore area is computationally feasible. Figure 27.5 gives an example of this hybrid simulation approach for nonlinear wind waves overtopping a coastal structure. The wind waves propagate from offshore with the Boussinesq model. Approximately one wavelength offshore of the break point, the Boussinesq and RANS models are two-way coupled, giving the ability for high resolution of the wave overtopping and a relatively large domain.

27.4 Summary of Model Properties

Table 27.1 provides a descriptive listing of the various models described in this chapter. Included in the table are typical spatial and temporal extents used in simulations along with resolutions, the number of derivatives operators found in the governing equations, and common applications and outputs. The information in the derivative operators column, which also includes the highest order of differentiation, is

Table 27.1 Summary of model types, with basic information for comparison purposes

Theory	Typical spatial domain sizes and spatial resolution	Typical simulation time coverage and time step	Number of derivative operators on unknowns in governing equations and highest derivative order	Typical applications and output types
Spectral wave energy balance equations	From planet-wide domains at ≈ 30 arcmin resolution to $O(100)$ km^2 at $O(100)$m resolution	Hours of simulation time with time steps of $O(5)$min	Four derivatives per frequency, with ≈ 250 frequencies. All derivatives are first order	Global scale operational wave prediction, coastal wave prediction, and wave drivers for nearshore circulation models. Models provide frequency-directional spectra
Phase-resolving nonlinear frequency domain equations	$O(1)$km^2 domains at $O(1)$m resolution	Hours, though dependent on number of frequencies retained. Time periodic models – no time step	Two derivatives per frequency, with 150–300 frequencies. Highest derivative order is 2	Nearshore and surf zone wave prediction, wave drivers for nearshore circulation models and models of instantaneous sediment transport. Models provide complex (phase-dependent) amplitudes of free surface elevation
Nonlinear shallow water (NSW) equations	From planet-wide domains at ≈ 2 arcmin resolution to $O(100)$km^2 domains at $O(10)$m resolution	Hours to multiple days of simulation time with time steps of $O(1)$ s	Approximately 10 in the 2DH formulation, depending on the specific formulation. All derivatives are first order	Coastal circulation modeling, tides, river and overland flows, tsunamis. Model provides water surface elevation and depth-averaged velocity components
Boussinesq-type equations	$O(1)$km^2 domains at $O(1)$m resolution	Tens of minutes to a few hours, with time steps of $O(0.1)$ s	Approximately 15 in the 2DH weakly nonlinear, standard formulations, with highest derivative order of 3. In the highly nonlinear 2DH versions, approximately 50, with highest derivative order of 3	Coastal wave prediction, breaking waves, setup, runup, overtopping, and coastal flooding due to waves. Model provides water surface elevation and velocity components at some z-level, which can be post-processed to construct the vertical profile of velocity
Navier–Stokes (NS) equations	Coastal applications currently focus on transect (2DV) studies, covering $O(1)$km of horizontal length, with depths less than 10 m. Horizontal resolutions are $O(1)$m and vertical resolutions are $O(0.1)$m	Tens of minutes to a few hours, with time steps of $O(0.01)$ s	Approximately 40 in the 2DV RANS equations with standard k-e turbulence closure model. Highest derivative order is 2	Detailed coastal wave prediction, breaking wave dynamics, turbulence, pressure distributions, wave loads on structures, wave transmission through porous structures. Model provides velocity components and turbulence information throughout the water column

meant to provide a basis to compare the computational cost of the various models; this is a measure of the effort required to determine a solution at every model grid node at every time step. It is remarked that this table provides information relative to *typical* model usage, here meaning applications that might arise in engineering practice or on an operational level. Research-level applications push the domain sizes, resolutions, and applications well beyond the types given below.

27.5 Conclusions

In this chapter, we have provided a cursory overview of coastal wave modeling theory and methods. The information contained here provides a useful starting point for understanding the differences in the wide variety of approaches. Ultimately, the choice of model will be governed by the resources available for the study and the primary piece of physical information that requires estimation. If resources are light and a precise estimate of the wave conditions is not yet needed, as might be the case for a preliminary scoping analysis, linear wave theory may be an acceptable approach for coastal transformation. If accurate and relatively large-scale wave height and period information is the goal, spectral models will most likely be the best option, with the included level of nonlinearity and resolution controlled by the resources of the project. For studies requiring detailed, small-scale, and wave-resolved information, such as might be needed for critical infrastructure, a Boussinesq or Navier–Stokes approach is reasonable. It is reiterated that the background given here, in terms of the individual models discussed, does not represent the wealth of numerical modeling tools available to the international engineering community.

27.6 Nomenclature

η free surface elevation
H wave height
a wave amplitude
θ wave phase function
k wave number
ω angular frequency
L wavelength
T wave period
f wave frequency
g gravity
h water depth
c wave speed
u horizontal fluid particle velocity
H_o offshore wave height
K_S shoaling coefficient
K_R refraction coefficient
K_D diffraction coefficient
α wave angle of incidence
F wave energy flux
N time-dependent wave action density
S external wave forcing, source/sink term in spectral wave equations
C_b bottom friction coefficient
G functional form of wave energy sink
E local wave energy density
ε wave amplitude divided by water depth $= a/h$
μ wave number times water depth $= kh$

References

27.1 N. Lin, K. Emanuel, M. Oppenheimer, E. Vanmarcke: Physically based assessment of hurricane surge threat under climate change, Nat. Clim. Change **2**, 462–467 (2012)

27.2 R.G. Dean, R.A. Dalrymple: *Water Wave Mechanics for Engineers and Scientists* (Prentice Hall, Englewood Cliffs 1984)

27.3 US Army Corps of Engineers: Coastal Engineering Manual. Engineer Manual 1110-2-1100, http://chl.erdc.usace.army.mil/cem (2002), in 6 volumes

27.4 B. Raubenheimer, R.T. Guza, S. Elgar: Wave transformation across the inner surf zone, J. Geophys. Res. **101**(C11), 25589–25597 (1996)

27.5 W.R. Dally, R.G. Dean, R.A. Dalrymple: Wave height variation across beach of arbitrary profile, J. Geophys. Res. **90**(C6), 11917–11927 (1985)

27.6 J.A. Battjes, J.P.F.M. Janssen: Energy loss and set-up due to breaking of random waves, Proc. 16th Coast. Eng. Conf. (1978) pp. 569–587

27.7 E.B. Thornton, R.T. Guza: Transformation of wave height distribution, J. Geophys. Res. **88**, 5925–5938 (1983)

27.8 D.T. Resio: The estimation of wind-wave generation in a discrete spectral model, J. Phys. Oceanogr. **2**(4), 510–525 (1981)

27.9 H.L. Tolman: User manual and system documentation of WAVEWATCH-III. Version 1.15. NOAA/NWS/NCEP/OMB Technical Note 151, http://polar.ncep.noaa.gov/mmab/papers/tn151/OMB_151.pdf (1997)

27.10 G.J. Komen, L. Cavaleri, M. Donelan, K. Hasselmannn, S. Hasselmannn, P.A.E.M. Janssen: *Dynamics and Modeling of Ocean Waves* (Cambridge Univ. Press, Cambridge 1994)

27.11 S. Wornom, D.J.S. Welsh, K.W. Bedford: On coupling the SWAN and WAM wave models for accurate nearshore wave predictions, Coast. Eng. J. **43**(3), 161–201 (2001)

27.12 N. Booij, R.C. Ris, L.H. Holthuijsen: A third-generation wave model for coastal regions, Part I: Model description and validation, J. Geophys. Res. **104**(C4), 7649–7666 (1999)

27.13 K. Hasselmann, T.P. Barnett, E. Bouws, H. Carlson, D.E. Cartwright, K. Enke, J.A. Ewing, H. Gienapp, D.E. Hasselmann, P. Kruseman, A. Meerburg, P. Müller, D.J. Olbers, K. Richter, W. Sell, H. Walden: *Measurements of Wind–Wave Growth and Swell Decay During the Joint North Sea Wave Project (JONSWAP)* (Deutsches Hydrographisches Institut, Hamburg 1973)

27.14 L. Cavaleri, J.-H.G.M. Alves, F. Ardhuin, A. Babanin, M. Banner, K. Belibassakis, M. Benoit, M. Donelan, J. Groeneweg, T.H.C. Herbers, P. Hwang, P.A.E.M. Janssen, T. Janssen, I.V. Lavrenov, R. Magne, J. Monbaliu, M. Onorato, V. Polnikov, D. Resio, W.E. Rogers, A. Sheremet, J. McKee Smith, H.L. Tolman, G. van Vledder, J. Wolf, I. Young: Wave modelling – The state of the art, Prog. Oceanogr. **75**, 603–674 (2007)

27.15 W.E. Rogers, J.M. Kaihatu, H.A.H. Petit, N. Booij, L.H. Holthuijsen: Diffusion reduction in an arbitrary scale third generation wind wave model, Ocean Eng. **29**, 1357–1390 (2002)

27.16 J.M. Smith: Full-plane STWAVE with bottom friction: II. Model overview. CHETN-I-75, http://chl.erdc.usace.army.mil/chetn (2007)

27.17 J.T. Kirby, R.A. Dalrymple: A parabolic equation for the combined refraction-diffraction of Stokes waves by mildly varying topography, J. Fluid Mech. **136**, 453–466 (1983)

27.18 J.T. Kirby, R.A. Dalrymple: *Combined Refraction/Diffraction Model REF/DIF 1, Version 2.5. Documentation and User's Manual*, Vol. Res. Rep. No. CACR-94-22 (Center for Applied Coastal Research, Department of Civil Engineering, University of Delaware, Newark 1994)

27.19 M.H. Freilich, R.T. Guza: Nonlinear effects on shoaling surface gravity waves, Philos. Trans. R. Soc. A **311**, 1–41 (1984)

27.20 Y. Agnon, A. Sheremet, J. Gonsalves, M. Stiassnie: Nonlinear evolution of a unidirectional shoaling wave field, Coast. Eng. **20**, 29–58 (1993)

27.21 J.M. Kaihatu, J.T. Kirby: Nonlinear transformation of waves in finite water depth, Phys. Fluids **7**, 1903–1914 (1995)

27.22 T.T. Janssen, T.H.C. Herbers, J.A. Battjes: Generalized evolution equations for nonlinear surface gravity waves over two-dimensional topography, J. Fluid Mech. **552**, 393–418 (2006)

27.23 J.M. Kaihatu: Frequency domain models in the nearshore and surf zones. In: *Advances in Coastal Modeling*, ed. by V.C. Lakhan (Elsevier, Amsterdam 2003)

27.24 J.M. Kaihatu: Improvement of parabolic nonlinear dispersive wave model, J. Waterw. Port Coast. Ocean Eng. **127**, 113–121 (2001)

27.25 Y. Agnon, A. Sheremet: Stochastic nonlinear modeling of directional spectra, J. Fluid Mech. **345**, 79–99 (1997)

27.26 J.M. Kaihatu, J. Veeramony, K.L. Edwards, J.T. Kirby: Asymptotic behavior of frequency and wavenumber spectra of nearshore shoaling and breaking waves, J. Geophys. Res. **112**, C06016 (2007)

27.27 T.H.C. Herbers, M.C. Burton: Nonlinear shoaling of directionally spread waves on a beach, J. Geophys. Res. **102**, 21101–21114 (1997)

27.28 D. Peregrine: Long waves on a beach, J. Fluid Mech. **27**(4), 815–827 (1967)

27.29 S. Elgar, R.T. Guza: Shoaling gravity waves: A comparison between data, linear finite depth theory and a nonlinear model, J. Fluid Mech. **158**, 47–70 (1985)

27.30 D.G. Goring: Tsunamis – The Propagation of Long Waves Onto a Shelf, Ph.D. Thesis (California Institute of Technology, Pasadena 1978)

27.31 P.L.-F. Liu, S.B. Yoon, J.T. Kirby: Nonlinear refraction-diffraction of waves in shallow water, J. Fluid Mech. **153**, 184–201 (1985)

27.32 O. Nwogu: Alternative form of Boussinesq equations for nearshore wave propagation, J. Waterw. Port Coast. Ocean Eng. **119**(6), 618–638 (1993)

27.33 P.A. Madsen, R. Murray, O.R. Sørensen: A new form of the Boussinesq equations with improved linear dispersion characteristics (Part 1), Coast. Eng. **15**, 371–388 (1991)

27.34 Y. Chen, P.L.-F. Liu: The unified Kadomtsev-Petviashvili equation for interfacial waves, J. Fluid Mech. **288**, 383–408 (1995)

27.35 J.M. Witting: A unified model for evolution of nonlinear water waves, J. Comput. Phys. **56**, 203–236 (1984)

27.36 Q. Chen, P.A. Madsen, H.A. Schaffer, D.R. Basco: Wave-current interaction based on an enhanced Boussinesq approach, Coast. Eng. **33**, 11–39 (1998)

27.37 P.L.-F. Liu: Model equations for wave propagation from deep to shallow water. In: *Advances in Coastal and Ocean Engineering*, Vol. 1, ed. by P.L.-F. Liu (World Sciectific, Singapore 1994)

27.38 G. Wei, J.T. Kirby, S.T. Grilli, R. Subramanya: A fully nonlinear Boussinesq model for surface waves. I. Highly nonlinear, unsteady waves, J. Fluid Mech. **294**, 71–92 (1995)

27.39 P. Lynett, P.L.-F. Liu: A numerical study of submarine landslide generated waves and runup, Proc. R. Soc. Lond. A **458**, 2885–2910 (2002)

27.40 Q. Chen, R.A. Dalrymple, J.T. Kirby, A. Kennedy, M.C. Haller: Boussinesq modeling of a rip current system, J. Geophys. Res. **104**(C9), 20617–20637 (1999)

27.41 Q. Chen, J.T. Kirby, R.A. Dalrymple, F. Shi, E.B. Thornton: Boussinesq modeling of longshore currents, J. Geophys. Res. **108**(C11), 3362 (2001)
27.42 P. Lynett, T.-R. Wu, P.L.-F. Liu: Modeling wave runup with depth-integrated equations, Coast. Eng. **46**(2), 89–107 (2002)
27.43 S. Ryu, M.H. Kim, P. Lynett: Fully nonlinear wave-current interactions and kinematics by a bem-based numerical wave tank, Comput. Mech. **32**, 336–346 (2003)
27.44 J. Veeramony, I.A. Svendsen: The flow in surf zone waves, Coast. Eng. **39**, 93–122 (2000)
27.45 R.E. Musumeci, I.A. Svendsen, J. Veeramony: The flow in the surf zone: A fully nonlinear Boussinesq-type of approach, Coast. Eng. **52**(7), 565–598 (2005)
27.46 D.-H. Kim, P.J. Lynett, S.A. Socolofsky: A depth-integrated model for weakly dispersive, turbulent, and rotational fluid flows, Ocean Model. **27**(3/4), 198–214 (2009)
27.47 D.H. Kim, P.J. Lynett: Turbulent mixing and scalar transport in shallow and wavy flows, Phys. Fluids **23**, 016603 (2011)
27.48 K. Sitanggang, P. Lynett: Parallel computation of a highly nonlinear Boussinesq equation model through domain decomposition, Int. J. Numer. Methods Fluids **49**(1), 57–74 (2005)
27.49 P. Lin, P.L.-F. Liu: Turbulent transport, vorticity dynamics, and solute mixing under plunging breaking waves in surf zone, J. Geophys. Res. **103**(C8), 15677–15694 (1998)
27.50 P. Lin, P.L.-F. Liu: A numerical study of breaking waves in the surf zone, J. Fluid Mech. **359**, 239–264 (1998)
27.51 T.-J. Hsu, T. Sakakiyama, P.L.-F. Liu: A numerical model for wave motions and turbulence flows in front of a composite breakwater, Coast. Eng. **46**(1), 25–50 (2002)
27.52 Q. Zhao, S. Armfield, K. Tanimoto: Numerical simulation of breaking waves by a multi-scale turbulence model, Coast. Eng. **51**(1), 53–80 (2004)
27.53 J.L. Lara, I.J. Losada, M. Maza, R. Guanche: Breaking solitary wave evolution over a porous underwater step, Coast. Eng. **58**(9), 837–850 (2011)
27.54 N. Garcia, J.L. Lara, I.J. Losada: 2-D numerical analysis of near-field flow at low-crested permeable breakwaters, Coast. Eng. **51**(10), 991–1020 (2004)
27.55 A. Pedrozo-Acuña, A. Torres-Freyermuth, Q. Zou, T.-J. Hsu, D.E. Reeve: Diagnostic investigation of impulsive pressures induced by plunging breakers impinging on gravel beaches, Coast. Eng. **57**(3), 252–266 (2010)
27.56 OpenFoam: The OpenSource CFD toolbox, User guide, Version 1.4.1., http://www.openfoam.org/docs (2007)
27.57 P. Higuera, J.L. Lara, I.J. Losada: Realistic wave generation and active wave absorption for Navier–Stokes models: Application to OpenFOAM, Coast. Eng. **71**, 102–118 (2013)
27.58 C. Dawson, J.J. Westerink, J.C. Feyen, D. Pothina: Continuous, discontinuous and coupled discontinuous-continuous Galerkin finite element methods for the shallow water equations, Int. J. Numer. Methods Fluids **52**, 63–88 (2006)
27.59 WL|Delft Hydraulics: Delft3D-FLOW User Manual, Version 3.13., http://www.oss.deltares.nl/web/delft3d/manuals (2006), 638p.
27.60 J. Dietrich, S. Tanaka, J.J. Westerink, C.N. Dawson, R.A. Luettich Jr, M. Zijlema, L.H. Holthuijsen, J.M. Smith, L.G. Westerink, H.J. Westerink: Performance of the unstructured-mesh, SWAN+ADCIRC model in computing hurricane waves and surge, J. Sci. Comput. **52**(2), 468–497 (2012)
27.61 V.V. Titov, C.E. Synolakis: Numerical modeling of tidal wave runup, J. Waterw. Port Coast. Ocean Eng. **124**(4), 157–171 (1998)
27.62 P.L.-F. Liu, Y.-S. Cho, S.B. Yoon, S.N. Seo: Numerical simulations of the 1960 Chilean tsunami propagation and inundation at Hilo, Hawaii. In: *Recent Development in Tsunami Research*, ed. by M.I. El-Sabh (Kluwer, Dordrecht 1994) pp. 99–115
27.63 F. Imamura, N. Shuto, C. Goto: Numerical simulations of the transoceanic propagation of tsunamis, Proc. 6th Cong. Asian Pac. Reg. Div. (IAHR) (1988) pp. 265–272
27.64 L. Mansinha, D.E. Smylie: The displacement fields of inclined faults, Bull. Seismol. Soc. Am. **61**, 1433–1440 (1971)
27.65 Y. Okada: Surface deformation due to shear and tensile faults in a half-space, Bull. Seism. Soc. Am. **75**(4), 1135–1154 (1985)
27.66 H. Kanamori: The energy release in great earthquakes, J. Geophys. Res. **82**, 2981–2987 (1977)
27.67 S.T. Grilli, M. Ioualalen, J. Asavanant, F. Shi, J.T. Kirby, P. Watts: Source constraints and model simulation of the December 26, 2004 Indian Ocean tsunami, J. Waterw. Port Coast. Ocean Eng. **133**, 414–428 (2007)
27.68 P. Lynett: Nearshore modeling using high-order Boussinesq equations, J. Waterw. Port Coast. Ocean Eng. **132**(5), 348–357 (2006)
27.69 S. Son, P. Lynett, D.-H. Kim: Nested and multi-physics modeling of tsunami evolution from generation to inundation, Ocean Model. **38**(1/2), 96–113 (2011)
27.70 S. Guignard, S. Grilli, R. Marcer, V. Rey: Computation of shoaling and breaking waves in nearshore areas by the coupling of BEM and VOF methods, Proc. 9th Offshore Polar Eng. Conf., Vol. 3 (1999) pp. 304–309
27.71 K. Sitanggang, P. Lynett: Multi-scale simulation with a hybrid Boussinesq-RANS hydrodynamic model, Int. J. Numer. Methods Fluids **62**, 1013–1046 (2009)